Interface Adhesion between 2D Materials and Elastomers Measured by Buckle Delaminations

*Christopher J. Brennan, Jessica Nguyen, Edward T. Yu, and Nanshu Lu**

2D systems have great promise as next generation electronic materials but require intimate knowledge of their interactions with their neighbors for device fabrication and mechanical manipulation. Although adhesion between 2D materials and stiff substrates such as silicon and copper has been measured, adhesion between 2D materials and soft polymer substrates remains difficult to characterize due to the large deformability of the polymer substrates. In this work, a buckling-based metrology for measuring the adhesion energy between few layer molybdenum disulfide (MoS_2) and soft elastomeric substrates is proposed and demonstrated. Due to large elastic mismatch, few layer MoS_2 flakes can form spontaneous wrinkles and buckle-delaminations on elastomer substrates during exfoliation. MoS_2-elastomer interface toughness can therefore be calculated from the buckle delamination profile measured by atomic force microscopy. The thickness of the MoS_2 flake is obtained by analyzing coexisting wrinkles on the same flake. Using this approach, adhesion of few layer MoS_2 to 10:1 Sylgard 184 polydimethylsiloxane is measured to be 18 ± 2 mJ m^{-2}, which is about an order of magnitude below graphene-to-stiff-substrate adhesion. Finally, this simple methodology can be generalized to obtain adhesion energies between various combinations of 2D materials and deformable substrates.

1. Introduction

Interest in 2D materials has grown quickly due to their low profile,[1] high deformability,[2] visual transparency,[3] and superior electronic performance.[4] Potential applications of 2D materials include transparent electronics,[5] chemical sensors,[6] and flexible electronics.[7] With the emergence of stretchable electronics[8,9] and biointegrated electronics,[10,11] many more opportunities for 2D materials await to be explored.

C. J. Brennan, J. Nguyen, Prof. E. T. Yu
Microelectronics Research Center and the
Department of Electrical and Computer Engineering
The University of Texas at Austin
Austin, TX 78758, USA
Prof. N. Lu
Center for Mechanics of Solids
Structures and Materials
Department of Aerospace Engineering and Engineering Mechanics
Texas Materials Institute
The University of Texas at Austin
Austin, TX 78712, USA
E-mail: nanshulu@mail.utexas.edu

DOI: 10.1002/admi.201500176

In general, fabrication of 2D electronic systems involves transferring the 2D material from one substrate to another in a process called transfer printing.[12,13] This process relies heavily on the interactions between the 2D material and the various surfaces that it contacts. Adhesion values must allow for the transfer from one substrate to another. By gaining a better understanding of the adhesion energy between 2D materials and the various substrates involved, the transfer process can be improved to allow for the picking up and printing of 2D materials onto arbitrary flexible and stretchable substrates.

Adhesion of 2D materials is also a controlling parameter for device mechanics. As a component in an integrated device, a 2D material will have to make secure contact with supporting substrates, metallic interconnects, other 2D materials, encapsulation layers, and other elements of a complete system. The mechanical interaction between 2D materials and their neighbors is an important parameter that governs the mechanical integrity of the device during thermal and mechanical loadings. Mechanical loading is often prominent during the operation of flexible 2D devices. For example, strain engineering of 2D materials on polymer substrates can be achieved by deforming the substrate,[14] but any slippage between 2D materials and the substrate would weaken the strain transfer to the 2D materials and hence limit the tunability. Moreover, slippage between 2D materials and their polymer substrates when the substrate is deformed may lead to buckle delaminations or wrinkles when the substrate is unloaded,[15] resulting in device degradation.

Because of the significance of adhesion, many experimental studies have been carried out to measure the adhesion energy between graphene and stiff substrates, as summarized in a recent review paper.[16] For example, adhesion energy between exfoliated monolayer graphene and SiO_2 has been measured to be 450 mJ m^{-2} by a pressurized blister method,[17] while adhesion of chemical vapor deposited (CVD) monolayer graphene to Si measured by double cantilever peeling method is found to be 357 mJ m^{-2}. Adhesion between CVD graphene and seed copper has been measured to be 720 mJ m^{-2} using cantilever method[18] whereas after transferring CVD graphene to a foreign copper surface, the interface adhesion was found to be only 510 mJ m^{-2} using a blister test.[19]

© 2015 WILEY-VCH Verlag GmbH & Co. KGaA, Weinheim

Adhesion between graphene and stretchable substrates is much less investigated due to the difficulty of handling soft substrates, with only two attempts reported so far. First, the lower bound of the adhesion energy between exfoliated graphene and polydimethylsiloxane (PDMS) elastomer has been estimated to be 7 mJ m^{-2} by probing the conformability of exfoliated graphene on a precorrugated PDMS surface.[20] Second, the adhesion energy between exfoliated graphene and a polyethylene terephthalate (PET) substrate has been estimated to be 0.54 mJ m^{-2} from buckling analysis, but the buckle profile measured by the atomic force microscope (AFM) is of low resolution in this work and the authors called for more accurate experiments.[21]

Buckling and wrinkling are instability phenomena often observed when stiff membranes are bonded to compliant substrates,[22] and have been harnessed to create stretchable electronics out of intrinsically brittle, inorganic semiconductor nanoribbons,[23–25] and graphene.[26,27] In addition, wrinkle-based metrology has been applied to probe the mechanical properties of thin films[28,29] and buckle-delamination-based metrology has been used to measure film-to-substrate adhesion.[30–32] In this work we apply both wrinkle-based and buckle-delamination-based metrologies on 2D materials bonded to soft elastomeric substrates. In our process, concomitant wrinkles and buckle delaminations can be created in the same MoS_2 flake exfoliated onto a PDMS substrate. Fitting the buckle delamination profile allows for the calculation of the adhesion between the MoS_2 and the PDMS, but requires very accurate knowledge of the width and height of the buckle delamination as well as the thickness of the MoS_2 flake. Instead of using an AFM step height measurement or Raman spectroscopy, fitting the wrinkle profile can yield more accurate flake thicknesses. Applying these two metrologies on the same MoS_2 flake provides a very simple but reliable process to calculate the adhesion between few layer MoS_2 and PDMS.

2. Results and Discussion

Buckle delaminations are created in a processes we will refer to as spontaneous buckling, shown in **Figure 1**, so named because little processing is required beyond finger indentation during the 2D material transfer step. The conventional process of creating buckles by prestretching the substrate before the transfer step[33] was also attempted, but cases in which delaminations and wrinkles coexisted were not observed, so accurate thickness measurements could not be performed. Exfoliation of the MoS_2 is done by pressing down firmly on the PDMS during the transfer process, after which some buckle delaminations and wrinkles would appear. The proposed mechanism for the buckle formation is that pressing down and creating an indent in the PDMS results in a slight local surface expansion (Figure 1a). When the pressure is released, the substrate relaxes and the MoS_2 flake adhered to the PDMS experiences an effective compressive force leading to buckle instability and sometimes concurrent wrinkle and buckle delamination formation (Figure 1b). The characteristic geometric parameters for buckle delaminations and wrinkles are labeled in Figures 1c,d, respectively.

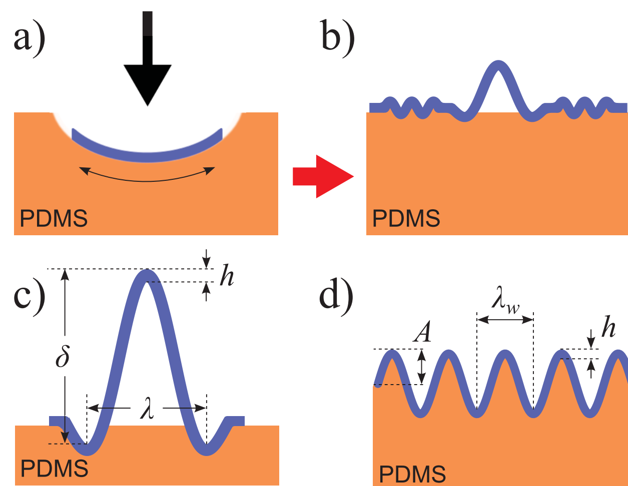

Figure 1. Schematics of the process to create spontaneous wrinkles and buckle delaminations in few layer MoS_2 on PDMS substrate. a) Surface expansion induced by finger indentation when exfoliating few layer MoS_2 on PDMS. b) Spontaneous wrinkles and buckle delaminations may form on the same flake when pressure was released. c) The definition of flake thickness, h, delamination height, δ, and delamination width, λ. d) The definition of wrinkle amplitude (half of peak-to-peak), A, and wrinkle wavelength λ_w. Note that delaminations and wrinkles are not drawn to scale.

Figure 2a shows an optical microscope image of a few-layer MoS_2 flake on a PDMS substrate created using the spontaneous buckling method. Buckle delaminations can be seen as dark lines running across the sample and wrinkles appear adjacent to the buckle delaminations as fainter, more tightly packed lines. Figure 2b shows the Raman spectrum of the same MoS_2 flake on the PDMS substrate. There is a separation of 22.2 cm^{-1} between the E^1_{2g} and the A_{1g} peaks, which is typically indicative of greater than 3 layers of MoS_2.[34] However, there is a possibility that there is some residual compressive strain in the flat regions of the MoS_2 which was not completely relaxed by the

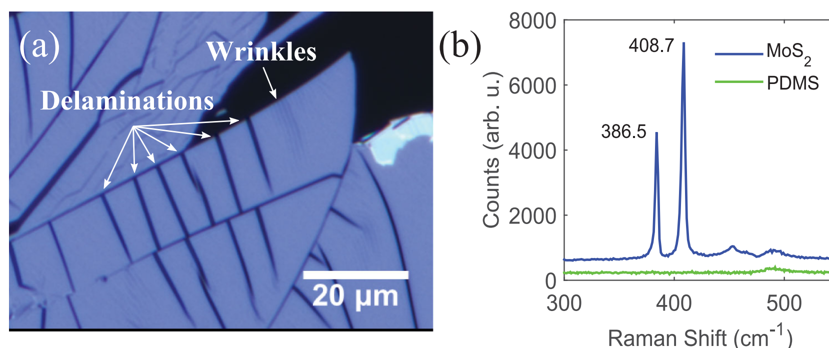

Figure 2. a) Optical image of an MoS_2 flake exfoliated on a PDMS substrate. Delaminations appear as isolated dark lines running across the MoS_2 surface and wrinkles appear as fainter lines in a periodic pattern running parallel to the delaminations. b) Raman spectra of bare PDMS and MoS_2 flake on PDMS as shown in (a).

© 2015 WILEY-VCH Verlag GmbH & Co. KGaA, Weinheim

buckling and wrinkling. The presence of strain in the MoS_2 flake would result in a shift of the peak separation.[35,36] Additionally, as the MoS2 flake increases in its number of layers, the peak separation shift becomes less sensitive and approaches that of the bulk. The samples presented here have thicknesses where the peak separation shift only changes slightly when adding or removing a single layer.[34] The combination of Raman insensitivity for thicker flakes (4+ layers) and the possible presence of strain make Raman spectroscopy a suboptimal method of determining thickness in this case. The background signal of PDMS is displayed in green to show that there is no overlap with the MoS_2 Raman peaks. Transmission mode optical images were also taken in an attempt to determine the number of layers present, but issues in accurately measuring the contrast differences between the number of layers resulted in abandoning this method.

When buckle delamination occurs, linear elastic fracture mechanics offers a simple formula to calculate the adhesion energy, also known as the interface toughness, between the buckled film and the underlying substrate from the buckling profile as[32]

$$\Gamma = 2\pi^4 \frac{B\delta^2}{\lambda^4}, \tag{1}$$

where Γ is the adhesion energy, B is the bending stiffness of the film, δ is the delamination height, and λ is the delamination width. Conveniently, this equation does not depend on the compressive strain that induced the buckles. Substituting $B = \bar{E}{*}h^3/12$ where h is the film thickness and $\bar{E}$ is the plane strain modulus defined as $\bar{E} = E/(1-\nu^2)$, where E and ν are the Young's modulus and Poisson's ratio of the film, respectively, the interface toughness can be expressed in terms of the film thickness, buckle height, and buckle width as

$$\Gamma = \frac{\pi^4}{6}\frac{h^3\delta^2}{\lambda^4}\frac{E}{1-\nu^2}. \tag{2}$$

Since Γ scales with h^3, δ^2, and λ^{-4}, small measurement errors in h, δ, and λ can be significantly magnified due to error propagation.[37] Accurate measurement of h, δ, and λ is therefore critical for determination of Γ with minimal uncertainty. Since the mechanical properties of MoS_2 have already been measured[38,39] and simulated,[40] we simply obtain its Young's modulus E = 0.27 TPa[38] and Poisson's ratio ν = 0.25[40] from the literature.

Figure 3 shows AFM topographic images, and cross-sectional line profiles extracted from the images, of two MoS_2 samples containing both buckle delaminations and wrinkles. MoS_2

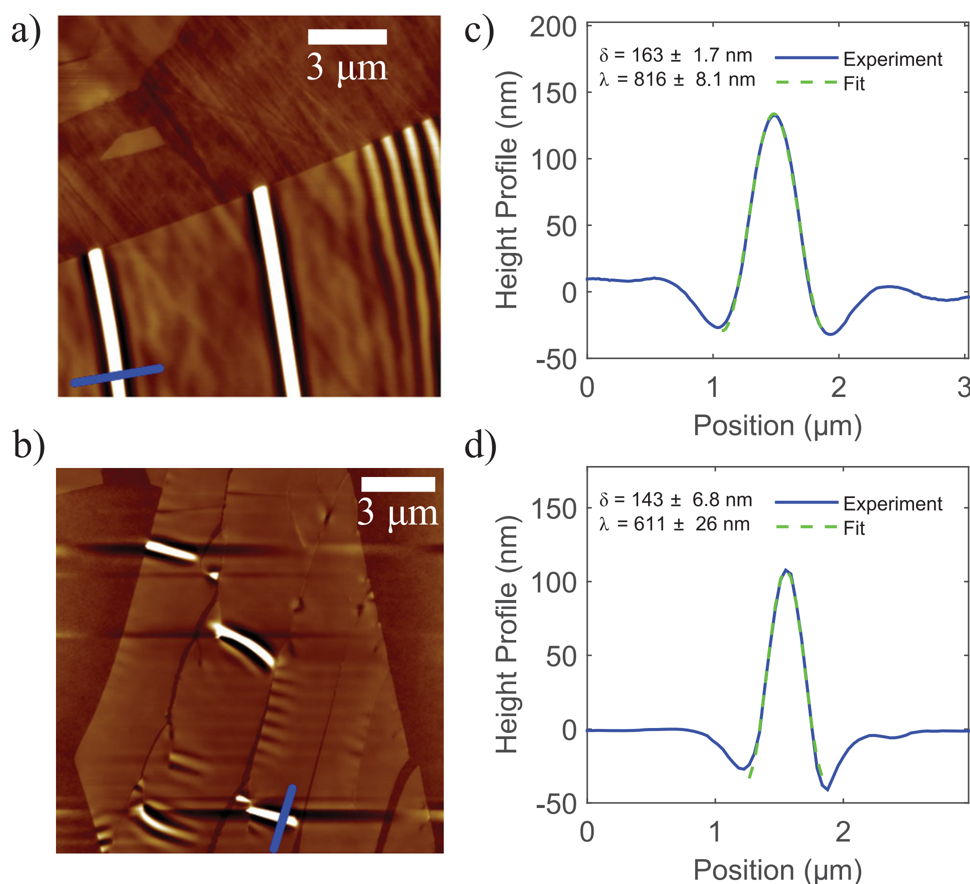

Figure 3. a,b) AFM images of MoS_2 flakes on PDMS. The isolated bright streaks indicate delaminations. c,d) Height profiles along the blue lines in (a) and (b) are fitted to a singular sinusoidal peak as represented by the dashed green curves. The extracted delamination height, δ, and width, λ, values along with uncertainties are given on the graph.

© 2015 WILEY-VCH Verlag GmbH & Co. KGaA, Weinheim

buckle delaminations and wrinkles are the same thickness because no layer steps between the features are seen in either the AFM or optical images. Buckle delaminations in MoS_2 flakes are distinguished from other features by their sinusoidally shaped peaks flanked on either side by smaller depressions, as illustrated in Figure 1c. They can also be seen in Figure 3a,b as bright streaks running across the MoS_2 flakes. Height profiles are taken from the AFM images for each single intersecting blue line in Figure 3a,b and shown in Figure 3c,d, respectively. The profiles are then fit to the buckle delamination profile[32]

$$d(x) = \frac{\delta}{2}\left(1 + \cos\frac{2\pi(x - x_{off})}{\lambda}\right) + y_{off}, \quad (3)$$

using a Matlab least-squares fitting function to obtain δ and λ. Here, $d(x)$ is the height at a given point x along the delamination cross-section, x_{off} and y_{off} are coordinate offsets, and the line thickness in the figures is for clarity and not to indicate averaging. The fits are shown by the dashed lines in Figure 3c,d and have almost perfect overlap with the actual curve.

Obtaining accurate measurements of film thickness, h, proved to be a more difficult task than simply taking a step height measurement using the AFM. The large elastic mismatch between the MoS_2 and the PDMS substrate results in an artificial increase in the AFM step height measurement compared to the actual thickness of the MoS_2 flake. Such effects have also been seen previously with MoS_2 on soft Gel-Films,[33] for which the MoS_2 thickness was estimated using a combination of Raman microscopy, photoluminescence (PL) spectroscopy, and transmittance measurements. Other concerns have been raised regarding the reliability of AFM step height measurements of graphene from materials that are much stiffer than PDMS, such as SiO_2,[41] suggesting that there may be some uncertainty in AFM measurements at the scale of few-layer 2D material thickness. Despite these issues, AFM scanning profiles of wrinkles and buckle delaminations within one MoS_2 flake are still reliable as long as there is no abrupt change of material stiffness.

To remedy this problem, we have used wrinkle-based metrology to determine the actual MoS_2 thickness. To be able to use this method, the extra requirement of having wrinkles and buckle delaminations coexist on the same MoS_2 flake must be met, and fortunately it is theoretically possible[42] and has been observed in multiple flakes. The thickness and the amount of prestrain present in the system at the time of transfer can then be calculated simultaneously by fitting the sinusoidal wrinkle profile. Wrinkles can be distinguished from buckle delaminations by their periodic sinusoidal shape as opposed to the singular sinusoidal peak. The amplitude, A, and wavelength, λ_w, of the wrinkled system subjected to a compressive strain ε_{pre} beyond the critical strain-to-wrinkle are captured by the post-buckling solutions[43]

$$A = \frac{A_0}{\sqrt{1+\varepsilon_{pre}}\,(1+\xi)^{1/3}}, \quad (4)$$

$$\lambda_w = \frac{\lambda_0}{(1+\varepsilon_{pre})(1+\xi)^{1/3}}, \quad (5)$$

respectively, and are labeled in Figure 1d. A_0 and λ_0 are the amplitude and period at the onset of wrinkling at a critical strain point and are given, respectively, as

$$A_0 = h\sqrt{\frac{\varepsilon_{pre}}{\varepsilon_c} - 1}, \quad (6)$$

$$\lambda_0 = 2\pi h\left(\frac{\bar{E}_f}{3\bar{E}_s}\right)^{1/3}, \quad (7)$$

where the critical strain of wrinkling is

$$\varepsilon_c = \frac{1}{4}\left(\frac{3\bar{E}_s}{\bar{E}_f}\right)^{2/3}. \quad (8)$$

In these equations, $\xi = 5\varepsilon_{pre}(1+\varepsilon_{pre})/32$, while $\bar{E}_f = 0.288$ TPa and $\bar{E}_s = 2.40$ MPa are the plane-strain modulus of MoS_2[38] and PDMS,[44] respectively. The plane-strain modulus is defined as $\bar{E} = E/(1\text{-}\nu^2)$. Therefore, h and ε_{pre} can act as two fitting parameters for Equations (4) and (5) when the wrinkle amplitude and wavelength are known.

Figure 4 shows wrinkles from the same two MoS_2 flakes as in Figure 3 with height profiles provided for the cuts along the blue lines, again with no averaging across the width of the line. The amplitude and wavelength values are determined using the same fitting procedure as for the buckle delaminations, except the data are fit to multiple periods of Equation (3) instead of just one and A is defined as one-half of the peak-to-peak amplitude. From these data the thickness of the two MoS_2 flakes shown in Figure 4a,b can be calculated using Equations (4)–(8) to be 3.83 ± 0.3 nm and 3.04 ± 0.3 nm, respectively.

These two values suggest that the two samples vary by a thickness of 0.79 nm, or about one monolayer of MoS_2.[5,34,45–48] The MoS_2 flake shown in Figure 4a is then 5–6 layers thick with a monolayer thickness of 0.77 nm or 0.64 nm, respectively, while the MoS_2 in Figure 4b is 4–5 layers thick with a monolayer thickness of 0.76 or 0.61 nm, respectively. All of these monolayer thicknesses are within the ranges of values given by different literature reports.[5,34,45–47] Studies looking into interlayer spacing of bulk MoS_2 flakes using methods other than AFM have reported values[45–47] of 0.60–0.65 nm with more recent studies converging on 0.65 nm.[46,47] When AFM step height measurements of monolayer MoS_2 are reported, thicknesses range from 0.6 to 0.9 nm,[5,34,48] tending to be on the larger side of this range. These discrepancies suggest that measured heights of monolayer MoS_2 flakes tend to be slightly larger than the interlayer distance and support that AFM step height measurements may not be sufficient for very accurate measurements of few-layer MoS_2 thickness.

The uncertainty in measured values of the parameters h, δ, and λ must be taken into consideration when determining adhesion values. For the delamination height and width, the uncertainty is taken to be the 95% confidence interval of the fitting process. For the thickness measurements, roughly half of the monolayer thickness, or 0.3 nm, is used for the measurement uncertainty. The values used for each variable and their associated uncertainties are shown in **Table 1**. The uncertainties for the three variables are then propagated through

© 2015 WILEY-VCH Verlag GmbH & Co. KGaA, Weinheim

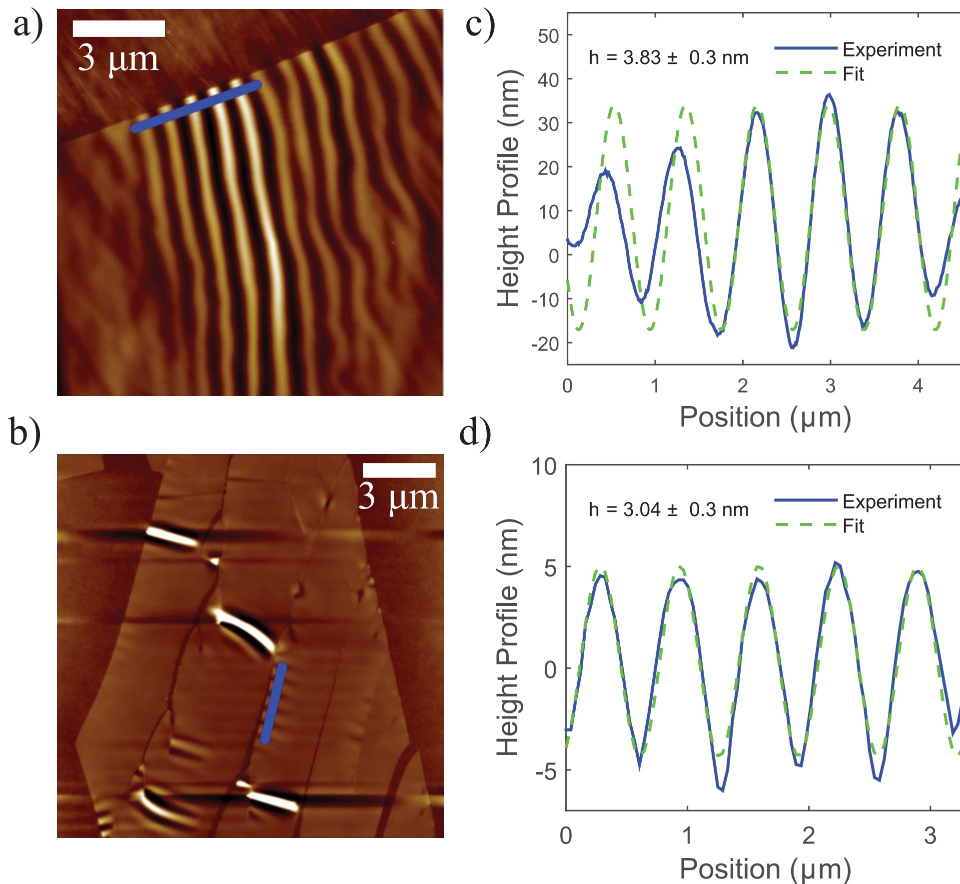

Figure 4. a,b) AFM images of the same two MoS_2 flakes shown in Figure 3a,b with a focus on the wrinkles. c,d) Height profiles along the blue lines given in (a) and (b) are fitted to a periodic sinusoidal curve as represented by the dashed green curves. The fit in (c) is performed on the data from the 3rd minima to the 6th minima of the graph and yields $A = 25.5$ nm and $\lambda_w = 814$ nm. The fit in (d) excludes the last minima graphed and yields $A = 4.7$ nm and $\lambda_w = 653$ nm. The thickness, h, as a fitting parameter is also given on the graph.

Equation (2) to obtain the total error in the adhesion by using the equation[37]

$$\sigma_\Gamma = \Gamma\sqrt{\left(\frac{3\sigma_h}{h}\right)^2 + \left(\frac{2\sigma_\delta}{\delta}\right)^2 + \left(\frac{4\sigma_\lambda}{\lambda}\right)^2 + \left(\frac{\sigma_E}{E}\right)^2}, \quad (9)$$

where σ_Γ, σ_h, σ_δ, σ_λ, and σ_E are uncertainties of the adhesion, MoS_2 thickness, delamination height, delamination width, and Young's modulus respectively. Equation (9) also incorporates the uncertainty of the Young's modulus of MoS_2 that currently exists in the literature, which is estimated to be ±0.06 TPa. Including the uncertainty of the Young's modulus, the total uncertainty increases by roughly 1 mJ m^{-2}. Additional uncertainty in the delamination height and width due to perturbation of the sample during the AFM measurement was analyzed and found to make a negligible contribution to the total experimental uncertainty and is therefore not included.

Table 1. Tabulated results of MoS_2 thickness, h, delamination height, δ, and delamination width, λ, which are used to calculate interface toughness using Equation (2). The uncertainties are also given on each measurement.

Delamination	h [nm]	δ [nm]	λ [nm]	Adhesion [mJ m^{-2}]
1	3.83 ± 0.3	163 ± 1.7	816 ± 8.1	16 ± 5
2	3.04 ± 0.3	143 ± 6.8	611 ± 26	19 ± 8
3	3.83 ± 0.3	188 ± 2.2	825 ± 8.1	20 ± 7
4	3.83 ± 0.3	213 ± 3.1	909 ± 9.2	17 ± 6
Average	–	–	–	18 ± 2

With all three geometric parameters in Equation (2) obtained through careful profile fittings, the adhesion of few-layer MoS_2 to PDMS can finally be calculated. Using the values given in Figures 3c,d and 4c,d, the adhesion of the first and second MoS_2 flakes are determined to be 16 ± 5 and 19 ± 8 mJ m^{-2}, respectively. Table 1 summarizes these values as well as those from two other measured delaminations not shown in Figures 3 and 4. Despite different flake thicknesses and buckling profiles, the four adhesion values are found to be very consistent. Averaging over four different delaminations, the adhesion between few-layer MoS_2 and PDMS is found to be 18 ± 2 mJ m^{-2} where the uncertainty is taken to be the standard deviation of the averaging process. This value is the first adhesion measurement of few-layer MoS_2 to a soft substrate and is higher than the lower bond found for graphene-PDMS interface (7 mJ m^{-2}).[20] More

© 2015 WILEY-VCH Verlag GmbH & Co. KGaA, Weinheim

work is needed to determine the dependence of adhesion on the number of MoS_2 layers, including monolayer MoS_2 which was not observed to show regular buckle-delaminations here.

To prove that our method is a generic one which can be applied to other similar systems, we also analyze a reported buckle delamination of MoS_2 on Gel-Film[33] where the height (380 ± 10 nm) and width (1100 ± 10 nm) of the buckle delamination are given on the profile. The uncertainty is added ad hoc here to account for any possible uncertainty in their measurements. Their estimate of 3–4 layers of MoS_2 is similar to the number of layers seen in our samples. Using a monolayer thickness of 6.7 Å and a relatively large uncertainty, the total thickness of their flake can be estimated to be ≈2.3 ± 0.6 nm. The adhesion calculated from the given values can then be estimated to be 6 ± 4.8 mJ m^{-2}, which is somewhat smaller than what we have measured between MoS_2 and PDMS.

3. Conclusion

A buckle-based metrology technique has been developed to measure the interface adhesion between 2D materials and elastomeric substrates. Taking advantage of the spontaneous and concomitant wrinkles and buckle delaminations that are formed when exfoliating MoS_2 on PDMS, the width and height of the delaminations can be easily extracted from the AFM scanning profile. The MoS_2 thickness, however, has to be determined through wrinkle analysis due to the deficiency of AFM step height measurements across materials with large elastic mismatch. The adhesion between few-layer MoS_2 and PDMS is measured to be 18 ± 2 mJ m^{-2}. This value is about an order of magnitude less than reported adhesion measurements between graphene and rigid substrates while being about an order of magnitude above reported estimates of adhesion between graphene and polymer substrates such as PDMS[20] and PET.[21] The implications of this measurement point toward possible device failure induced by slippage of 2D materials against polymer substrates when deforming 2D flexible electronics.[15] Although this paper focuses on MoS_2 to PDMS adhesion, the methodology is applicable to other systems involving 2D materials on soft substrates.

4. Experimental Section

PDMS Preparation: PDMS samples were created in our lab using the Sylgard 184 Silicone Elastomer kit in a 10:1 mixing ratio cured at 70 °C for 4 h. Typical local RMS surface roughness of the free surface of as-prepared PDMS slabs ranged from 1.0 to 2.3 nm as measured by AFM in the samples shown in this work. No pretreatment of the PDMS surface was done besides cleaning the surface with Scotch tape.

MoS_2 Exfoliation: Following the well-established exfoliation procedure for 2D layered materials,[34,35] a blue polyethylene cleanroom tape was used to peel large MoS_2 flakes off of a synthetic MoS_2 crystal obtained from 2D Semiconductors Inc.. Large flakes of many layers can be thinned downed with repeated exfoliations. Then the tape and thin MoS_2 flakes were pressed down onto the 10:1 PDMS by fingertips with enough force to create a visible indentation. When the indentation force was released and the tape rapidly peeled away, coexisting delaminations and wrinkles would appear in some of the MoS_2 flakes transferred to the PDMS.

Raman and Atomic Force Microscopy: A Renishaw inVia Raman microscope with a 532 nm laser was used for MoS_2 characterization and a Veeco/Bruker Dimension Icon AFM was used to obtain profiles of the buckle delaminations and wrinkles. AFM images were taken in tapping mode with a Bruker tapping-mode etched silicon probe (TESP) tip and with a minimum resolution of 25 samples μm^{-1} and a tip speed no faster than 32 $\mu m\ s^{-1}$. AFM imaging parameters were chosen to impart the lowest possible force onto the sample while still obtaining quality images. After applying different forces and extrapolating to a zero-force point, we estimate an uncertainty in the measurement of the buckle height and width of ±1% for each.

Acknowledgements

This work was supported by the NSF CMMI Award under Grant No. 1351875 and NSF DMR Award under Grant No. 1311866. E.T.Y. acknowledges the Judson S. Swearingen Regents Chair in Engineering at the University of Texas at Austin. C.J.B. acknowledges Dr. Brooks Carlton Fowler Endowed Presidential Graduate Fellowship in Electrical and Computer Engineering and the Temple Foundation Graduate Microelectronic and Computer Development Fellowship in Engineering of UT-Austin.

Received: April 8, 2015
Revised: July 19, 2015
Published online:

[1] A. K. Geim, K. S. Novoselov, *Nat. Mater.* **2007**, *6*, 183.
[2] K. S. Kim, Y. Zhao, H. Jang, S. Y. Lee, J. M. Kim, K. S. Kim, J.-H. Ahn, P. Kim, J.-Y. Choi, B. H. Hong, *Nature* **2009**, *457*, 706.
[3] F. Wang, Y. Zhang, C. Tian, C. Girit, A. Zettl, M. Crommie, Y. R. Shen, *Science* **2008**, *320*, 206.
[4] Y. Zhang, Y.-W. Tan, H. L. Stormer, P. Kim, *Nature* **2005**, *438*, 201.
[5] B. Radisavljevic, A. Radenovic, J. Brivio, V. Giacometti, A. Kis, *Nat. Nanotechnol.* **2011**, *6*, 147.
[6] E. W. Hill, A. Vijayaragahvan, K. Novoselov, *IEEE Sens. J.* **2011**, *11*, 3161.
[7] N. Petrone, J. Hone, D. Akinwande, *Nat. Commun.* **2015**, *5*, 1.
[8] J. A. Rogers, T. Someya, Y. Huang, *Science* **2010**, *327*, 1603.
[9] Z. Suo, *MRS Bull.* **2012**, *37*, 218.
[10] D.-H. Kim, R. Ghaffari, N. Lu, J. A. Rogers, *Annu. Rev. Biomed. Eng.* **2012**, *14*, 113.
[11] N. Lu, D.-H. Kim, *Soft Robot.* **2014**, *1*, 53.
[12] S. Bae, H. Kim, Y. Lee, X. Xu, J.-S. Park, Y. Zheng, J. Balakrishnan, T. Lei, H. R. Kim, Y. Il Song, Y.-J. Kim, K. S. Kim, B. Ozyilmaz, J.-H. Ahn, B. H. Hong, S. Iijima, *Nat. Nanotechnol.* **2010**, *5*, 574.
[13] J. W. Suk, A. Kitt, C. W. Magnuson, Y. Hao, S. Ahmed, J. An, A. K. Swan, B. B. Goldberg, R. S. Ruoff, *ACS Nano* **2011**, *5*, 6916.
[14] H. J. Conley, B. Wang, J. I. Ziegler, R. F. Haglund, S. T. Pantelides, K. I. Bolotin, *Nano Lett.* **2013**, *13*, 3626.
[15] H.-Y. Chang, S. Yang, J. Lee, L. Tao, W.-S. Hwang, D. Jena, N. Lu, D. Akinwande, *ACS Nano* **2013**, *7*, 5446.
[16] J. S. Bunch, M. L. Dunn, *Solid State Commun.* **2012**, *152*, 1359.
[17] S. P. Koenig, N. G. Boddeti, M. L. Dunn, J. S. Bunch, *Nat. Nanotechnol.* **2011**, *6*, 543.
[18] T. Yoon, W. C. Shin, T. Y. Kim, J. H. Mun, T.-S. Kim, B. J. Cho, *Nano Lett.* **2012**, *12*, 1448.
[19] Z. Cao, P. Wang, W. Gao, L. Tao, J. W. Suk, R. S. Ruoff, D. Akinwande, R. Huang, K. M. Liechti, *Carbon* **2014**, *69*, 390.
[20] S. Scharfenberg, D. Z. Rocklin, C. Chialvo, R. L. Weaver, P. M. Goldbart, N. Mason, *Appl. Phys. Lett.* **2011**, *98*, 091908.
[21] T. Jiang, R. Huang, Y. Zhu, *Adv. Funct. Mater.* **2014**, *24*, 396.
[22] N. Bowden, S. Brittain, A. Evans, *Nature* **1998**, *393*, 146.

© 2015 WILEY-VCH Verlag GmbH & Co. KGaA, Weinheim

[23] S. P. Lacour, S. Wagner, Z. Huang, Z. Suo, *Appl. Phys. Lett.* **2003**, *82*, 2404.
[24] D.-Y. Khang, H. Jiang, Y. Huang, J. A. Rogers, *Science* **2006**, *311*, 208.
[25] Y. Sun, W. M. Choi, H. Jiang, Y. Y. Huang, J. A. Rogers, *Nat. Nanotechnol.* **2006**, *1*, 201.
[26] J. Zang, S. Ryu, N. Pugno, Q. Wang, Q. Tu, M. J. Buehler, X. Zhao, *Nat. Mater.* **2013**, *12*, 321.
[27] Y. Wang, R. Yang, Z. Shi, L. Zhang, D. Shi, E. Wang, G. Zhang, *ACS Nano* **2011**, *5*, 3645.
[28] C. M. Stafford, C. Harrison, K. L. Beers, A. Karim, E. J. Amis, M. R. VanLandingham, H.-C. Kim, W. Volksen, R. D. Miller, E. E. Simonyi, *Nat. Mater.* **2004**, *3*, 545.
[29] E. A. Wilder, S. Guo, S. Lin-Gibson, M. J. Fasolka, C. M. Stafford, *Macromolecules* **2006**, *39*, 4138.
[30] A. Pundt, E. Nikitin, P. Pekarski, R. Kirchheim, *Acta Mater.* **2004**, *52*, 1579.
[31] M. J. Cordill, D. F. Bahr, N. R. Moody, W. W. Gerberich, *Mater. Sci. Eng. A* **2007**, *443*, 150.
[32] D. Vella, J. Bico, A. Boudaoud, B. Roman, P. M. Reis, *Proc. Natl. Acad. Sci. USA* **2009**, *106*, 10901.
[33] A. Castellanos-Gomez, R. Roldán, E. Cappelluti, M. Buscema, F. Guinea, H. S. J. van der Zant, G. A. Steele, *Nano Lett.* **2013**, *13*, 5361.
[34] C. Lee, H. Yan, L. E. Brus, T. F. Heinz, J. Hone, S. Ryu, *ACS Nano* **2010**, *4*, 2695.
[35] C. Rice, R. J. Young, R. Zan, U. Bangert, D. Wolverson, T. Georgiou, R. Jalil, K. S. Novoselov, *Phys. Rev. B: Condens. Matter Mater. Phys.* **2013**, *87*, 1.
[36] Y. Wang, C. Cong, C. Qiu, T. Yu, *Small* **2013**, *9*, 2857.
[37] P. R. Bevington, D. K. Robinson, *Data Reduction and Error Analysis for the Physical Sciences*, McGraw-Hill Book Company, Inc., New York **2003**.
[38] S. Bertolazzi, J. Brivio, A. Kis, *ACS Nano* **2011**, *5*, 9703.
[39] A. Castellanos-Gomez, M. Poot, G. A. Steele, H. S. J. van der Zant, N. Agraït, G. Rubio-Bollinger, *Adv. Mater.* **2012**, *24*, 772.
[40] K. Liu, Q. Yan, M. Chen, W. Fan, Y. Sun, J. Suh, D. Fu, S. Lee, J. Zhou, S. Tongay, J. Ji, J. B. Neaton, J. Wu, *Nano Lett.* **2014**, *14*, 5097.
[41] P. Nemes-Incze, Z. Osváth, K. Kamarás, L. P. Biró, *Carbon* **2008**, *46*, 1435.
[42] H. Mei, C. M. Landis, R. Huang, *Mech. Mater.* **2011**, *43*, 627.
[43] H. Jiang, D.-Y. Khang, J. Song, Y. Sun, Y. Huang, J. A. Rogers, *Proc. Natl. Acad. Sci. USA* **2007**, *104*, 15607.
[44] K. M. Choi, J. A. Rogers, *J. Am. Chem. Soc.* **2003**, *125*, 4060.
[45] R. F. Frindt, *J. Appl. Phys.* **1966**, *37*, 1928.
[46] K. S. Novoselov, D. Jiang, F. Schedin, T. J. Booth, V. V Khotkevich, S. V Morozov, A. K. Geim, *Proc. Natl. Acad. Sci. USA* **2005**, *102*, 10451.
[47] D.-M. Tang, D. G. Kvashnin, S. Najmaei, Y. Bando, K. Kimoto, P. Koskinen, P. M. Ajayan, B. I. Yakobson, P. B. Sorokin, J. Lou, D. Golberg, *Nat. Commun.* **2014**, *5*, 3631.
[48] A. Splendiani, L. Sun, Y. Zhang, T. Li, J. Kim, C.-Y. Chim, G. Galli, F. Wang, *Nano Lett.* **2010**, *10*, 1271.

© 2015 WILEY-VCH Verlag GmbH & Co. KGaA, Weinheim